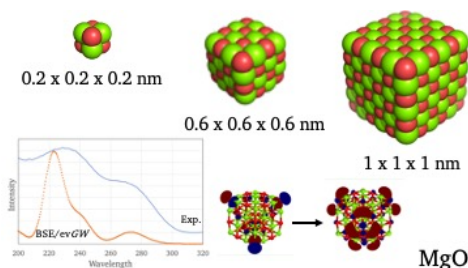# The Effect of Particle Size on the Optical and Electronic Properties of Magnesium Oxide Nanoparticles

Martijn A. Zwijnenburg

Department of Chemistry, University College London, 20 Gordon Street, London WC1H 0AJ, U.K.
Email: m.zwijnenburg@ucl.ac.uk

The (band) edge states, fundamental gaps, optical gaps, exciton binding energies and UV-Vis spectra for a series of cuboidal nanoparticles of the prototypical oxide magnesium oxide (MgO), the largest of with has 216 atoms and edges of 1 nm, were predicted using many-body perturbation theory (ev*GW*-BSE). The evolution of the properties with particle size was explicitly studied. It was found that while the edge states and fundamental gap change with particle size, the optical gap remains essentially fixed for all but the smallest nanoparticles, in line with what was previously observed experimentally. The explanation for these observations is demonstrated to be that while the optical gap is associated with an exciton that is highly localised around the particle's corner atoms, the edge states, while primarily localised on the magnesium corner atoms (electron) and oxygen corner atoms (hole), show significant delocalisation along the edges. The strong localisation of the exciton associated with the optical gap on the corner atoms is argued to also explain why the nanoparticles have a much smaller optical gaps and red-shifted spectra than bulk MgO. Finally, it is discussed how this non-quantum confinement behaviour, where the properties of the nanoparticles arise from surface defects rather than differences in localisation of edge or exciton states, appears typical of alkaline earth oxide nanoparticles, and that the true optical gap of bulk crystals of such materials is also probably the result of surface defects, even if unobservable experimentally.

Introduction

The effect of going from the bulk to nanosized particles on the optical and electronic properties of materials is interesting both from a fundamental and applied perspective.[1] Practically it offers an alternative way of tuning material properties besides changing composition while conceptually it raises questions about what exactly results in the properties of nanoparticles differing from those of the bulk. Quantum confinement,[2-3] where the size of the particle constrains the size of the exciton --the excited-electron hole pair formed by the absorption of light-- to a size smaller than in the bulk, is often invoked but requires the states involved to be delocalised over the particle, which is unlikely to be the case for more ionic materials. Quantum confinement also only explains blue-shifts with respect to the bulk, as *e.g.* observed for CdS,[4] CdSe,[5-6] PbS[7-8] and PBSe[9] nanoparticles, but not red-shifts, as *e.g.* observed for MgO,[10-11] CaO[11] and SrO[12] particles. An alternative mechanism by which the properties of nanoparticles may differ from the bulk involves the localisation of relevant states on low-coordinated surface atoms, which are ubiquitous on (small) nanoparticles. While experimental spectroscopy can clearly demonstrate the effect of nanostructuring on the electronic and optical properties, elucidating the atomic scale origin of these changes requires the combination of experiment with theory.

Magnesium oxide (MgO) nanoparticles are an ideal system to study differences in the optical and electronic properties between nanoparticles and the bulk and to synthesize the results of experiment and theory. Well-defined MgO nanoparticles as small as 3 nm have been prepared experimentally by means of chemical vapour deposition without the need for capping agents and found to display UV-Vis diffuse reflection and photoluminescence spectra that are significantly red-shifted relative to bulk magnesium oxide.[10-11] The lowest-energy most red-shifted exciton peak in the reflection spectrum of bulk MgO,[13-14] the bulk optical gap, is located at 7.7 eV (161 nm) while the lowest peak in the reflection spectrum of the 3 nm particles lies at ~4.6 eV (270 nm).[10] These 3 nm nanoparticles are confirmed to have the same rocksalt structure as bulk magnesium oxide, ruling out that the observed red shift is the result of major structural changes. Indeed, computational global optimisation studies show that in contrast to materials that in the bulk crystallise with the zincblende or wurtzite

structure, *e.g.* zinc or cadmium sulfide,[15-19] the lowest energy nanoparticles of materials that crystallise with the rocksalt structure, such as MgO,[20-22] are, even in the absence of capping agents, generally cuts from the that crystal structure. The fact that magnesium and oxygen are relatively light elements also means that relativistic effects including spin-orbit coupling will be small in MgO nanoparticles in contrast to other rocksalt nanoparticles, such as those made from PbS or PbSe. Interestingly, while the MgO nanoparticles' UV-Vis spectra are significantly red-shifted with respect to the bulk, the largest change in the diffuse reflectance spectra when changing the average particle size from 3 to 10 nm is not a shift in the peak positions but their relative intensities.[10]
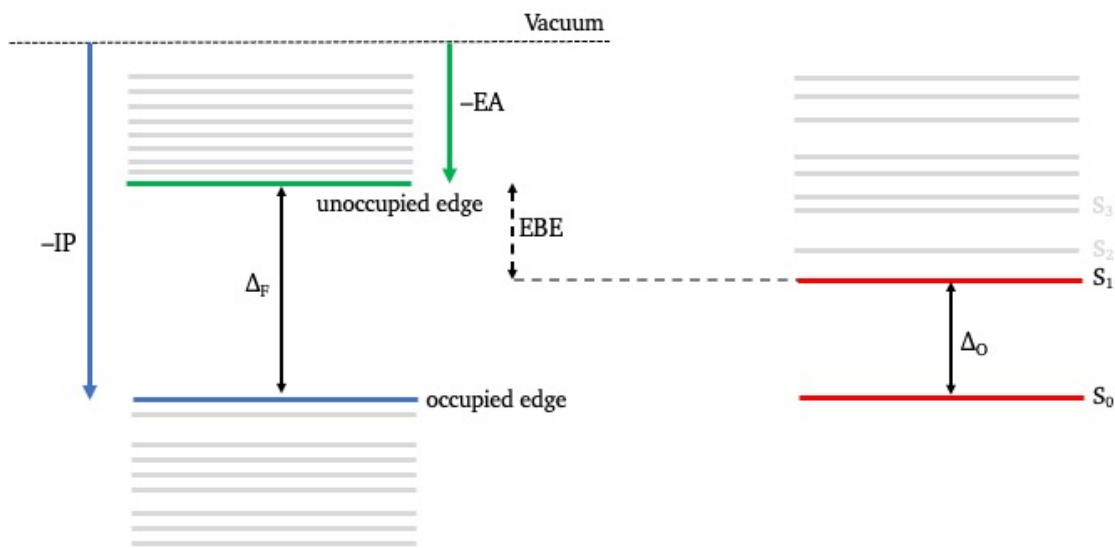

Fig. 1 Cartoon illustrating the definition of the occupied and unoccupied edge states (–IP and –EA), the fundamental gap (Δ_F), optical gap (Δ_O), and the exciton binding energy (EBE).

In contrast to the case of the optical properties, there appear to be no reports on the electronic structure of MgO nanoparticles: *i.e.* the fundamental gap, the energy required to generate a non-interacting excited electron and hole pair rather than an interacting exciton and/or the energies of the occupied (the negative of the ionisation potential, –IP) and unoccupied (the negative of the electron affinity, –EA) edge states (see Fig. 1). The latter concepts in the case of periodic crystals, where it is appropriate to speak of bands, map on to the bandgap, valence band maximum and conduction

band minimum, respectively. There are some reports in the literature of the fundamental gap narrowing for thin films of MgO.[23-24] However, as this is generally observed by means of electron energy loss spectroscopy (EELS) and as one of the loss mechanisms in EELS involves the generation of excitons, the feature at ~6 eV in the EELS spectrum of thin magnesium oxide films linked to the apparent narrowing of the fundamental gap in reality might be due to surface exciton formation[25] and thus be evidence of the narrowing of the thin films' optical gap instead.

The optical properties of MgO nanoparticles were previously studied[26-30] using time-dependent density functional theory (TD-DFT). The results of these TD-DFT calculations for whole nanoparticles was found to be rather sensitive to the exact density functional used[30] because of the well-known issue[31-32] of TD-DFT where charge-transfer excitations are spuriously stabilised with respect to local, *i.e.* non-charge-transfer, excitations. Well-chosen density functionals with the optimal amount of exact exchange can reproduce the key features of the experimental spectra of magnesium oxide nanoparticles: the red shift with respect to the bulk and the intensity change for the diffuse reflection peaks when changing particle size,[30] but the strong dependency on the amount of exact exchange makes these calculations more empirical than desirable. TD-DFT calculations using embedded cluster calculations[26-29] where only a region, *e.g.* a corner, of the nanoparticle is describe explicitly using TD-DFT and the effect of the rest of the particle on this region is described in terms of classical point charges, appear to be less sensitive to the functional choice, perhaps because many potential charge-transfer excitations, e.g. from oxygen corner atoms to magnesium corner atoms, are by definition absent in embedded cluster models.[30] It is however difficult to explicitly study the effect of particle size in embedded cluster calculations. An additional complication when using TD-DFT is that the optical gap and the UV-Vis spectra in general are not treated on the same footing as the particle's electronic properties. The edge states of a particle and its fundamental gap can in principle be calculated within the framework of ground state density functional theory (DFT) in two different ways, from the Kohn-Sham (KS) orbital energies or using ΔDFT. In the former case, the occupied and uncopied edge states map on to the highest occupied and lowest unoccupied KS orbitals and the fundamental gap on to the energy gap between these

two orbitals, the KS gap. In the latter case the energy of the occupied edge state is calculated from the difference in total energy between the neutral particle and the particle with one electron less, that of the unoccupied edge state from the total energy difference between the neutral particle and the particle with an extra electron, and the fundamental gap from the difference in energy between the unoccupied and occupied edge states. The ΔDFT approach is preferred as it can be shown that the KS gap, at least for pure density functionals, behaves more like the optical than the fundamental gap because the KS unoccupied orbitals feel the same field of N-1 electrons as the KS occupied orbitals instead of the correct N electrons.[33] However, regardless, it is not a given that the optimal density functional for calculating the spectra and optical gap values of particles is also optimal for calculating the particles' electronic properties. This is especially critical for properties such as the exciton binding energy, the difference between the fundamental and optical gap and a measure of how strongly excitons are bound (see Fig. 1), which span both worlds. ΔDFT predictions of edge state energies of MgO particles, including particles with defects or in the presence of grain boundaries, have previously been reported by Shluger and co-workers.[34-36]
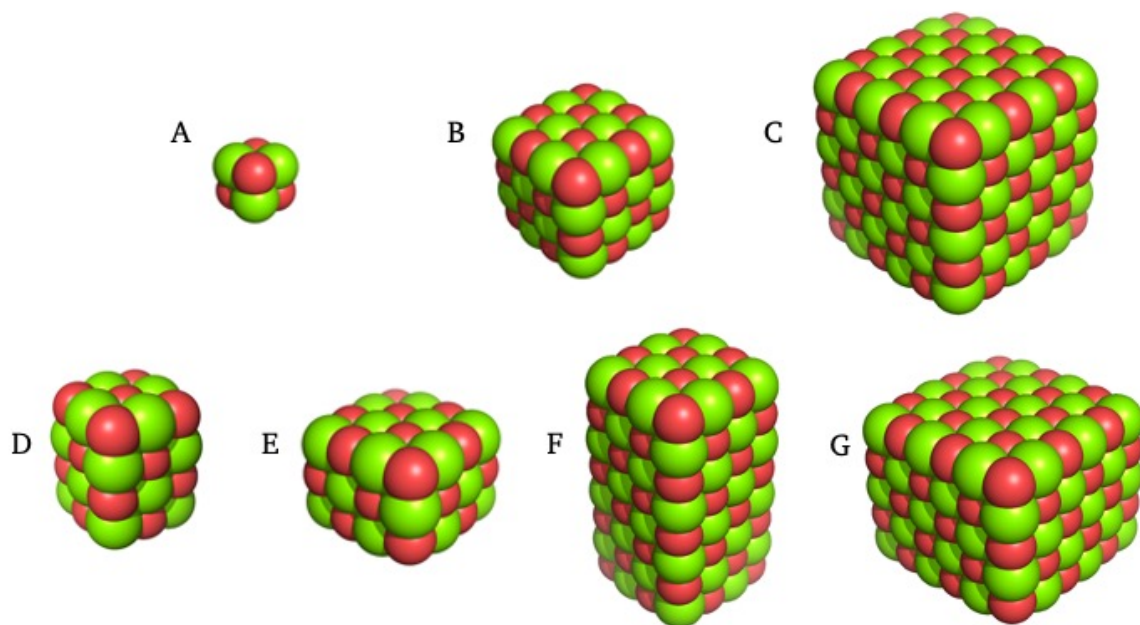
Fig. 2 Structures of some of the cuboidal particles studied. The cubes $(MgO)_4$ (A), $(MgO)_{32}$ (B) and $(MgO)_{108}$ (C), as well as the cuboids $(MgO)_{18}$ (D), $(MgO)_{24}$ (E), $(MgO)_{64}$ (F) and $(MgO)_{90}$ (G).

Here many-body perturbation theory, in the form of solving Hedin's *GW* equations[37-39] followed by the Bethe-Salpeter equation,[40-42] is used to calculate the optical and electronic properties of cuboidal MgO rocksalt nanoparticles, see Fig. 2, rather than (TD-)DFT. While computationally considerably more expensive than (TD-)DFT, *GW*-BSE has the advantage that it treats optical and electronic properties on a similar footing and that application of partial self-consistency in the *GW* part of the calculation, ev*GW*, removes most of the dependency on the specific density functional used in the underlying DFT calculation. Using *GW*-BSE the effect of particle size on the optical and fundamental gap of MgO nanoparticles, the localisation of the edge and excited state, as well as the excitonic character of the latter, is explored in order to explain the atomistic scale explanation of the differences between the nanoparticle properties and those of the bulk. The results are not only relevant to understand the properties of MgO nanoparticles but also lie the groundwork for future work on (rocksalt) nanoparticles of other materials.

Methodology

The geometry of the nanoparticles was optimised in DFT calculations, using the B3LYP[43-46] density functional in combination with the D3(BJ)[47-48] dispersion correction by Grimme and co-workers and either the def2-SVP or def2-TZVPP basis-set.[49] During the geometry optimisation the symmetry of the nanoparticles was fixed and for the smaller particles, up to and including $(MgO)_{32}$, frequency calculations were performed to verify that the optimised structures correspond to minima.

Single-shot G_0W_0, eigenvalue-only self-consistent *GW* (ev*GW*) and quasiparticle self-consistent (qsGW) calculations, as implemented by Holzer, van Setten, Klopper and co-workers in Turbomole,[50-52] were performed on the DFT optimised structures, starting from B3LYP orbitals and in selected case PBE[53] orbitals. These calculations used either the def2-SVP or def2-TZVPP basis-set (and in selected cases the def2-QZVPP and aug-cc-pVTZ basis-sets) and one of two *GW* implementations that differ in how the self-energy is obtained; in terms of a spectral representation (SR) or by analytical continuation (AC). The *GW* calculations using the spectral representation are the most computationally expensive, scaling as N^6, while the analytical continuation calculations are more computationally tractable, scaling as N^4. In the case of analytical continuation

only the two edge-states are explicitly calculated with *GW* and the rest of the orbitals simply shifted. The results of the different *GW* calculations are used as input for solving the BSE, again as implemented in Turbomole,[54] to obtain excitation energies and oscillator strength values. The character of the BSE excited-states is finally analysed in terms of the most prominent natural transition orbitals.[55] The same basis-sets are generally used for the geometry optimisation and the BSE-*GW* calculations, except where stated to the contrary.

For selected particles the lowest excitation energies are also calculated with LR-CCSD coupled-cluster theory on top of a Hartree-Fock ground-state. These correlated wavefunction calculations use either the def2-TZVPP or def2-QZVPP basis-set and are performed as single-point calculations on the DFT optimised geometry.

All calculations were performed using version 7.5 of the Turbomole code[56] and used a tight integration grid (m5) and tight SCF convergence criteria (scftol and denconv $1x10^{-7}$). All *GW* and BSE calculations additionally used the RI-K approximation and use of symmetry was limited to Abelian point groups. The *GW* and BSE calculations for $(MgO)_4$, $(MgO)_{32}$ and $(MgO)_{108}$, as well as $(CaO)_{32}$ and $(SrO)_{32}$, all of which have Td symmetry, were hence performed in the D_2 point group instead.

Results

(MgO)$_4$ and (MgO)$_{32}$.

First, the effect of the different *GW* approximations and implementations is studied by performing calculations on the smallest two perfect cubes, $(MgO)_4$ and $(MgO)_{32}$. Tables 1 and 2 give the edge states, fundamental gap, optical gap and exciton binding energy values predicted by the different method combinations for the two particles. Concentrating first on the effect of basis-set, with increasing basis-set size the edge states both move to deeper, more negative, values while the fundamental and optical gap increase and the exciton binding energy more or less remains the same. Generally, as would be expected, the shift when going from the triple-zeta def2-TZVPP to the quadruple-zeta def2-QZVPP basis-set is smaller than when going from def2-SVP to def2-TZVPP, except for the unoccupied edge state, for which the shift is similar. A

calculation using the augmented Dunning aug-cc-pVTZ basis-set, suggest that the effect of adding additional diffuse basis functions is minor.

Table 1 Occupied (–IP) and unoccupied (–EA) edge states, fundamental gap (Δ_F), optical gap (Δ_O) and exciton binding energy (EBE) values of $(MgO)_4$ as calculated by the different method combinations (TZVPP=def2-TZVPP, accTZ=aug-cc-pVTZ, QZVPP=def2-QZVPP, SVP=def2-SVP).

	G_0W_0					evGW				
	–IP	–EA	Δ_F	Δ_O	EBE	–IP	–EA	Δ_F	Δ_O	EBE
SR/TZVPP	-7.807	-0.518	7.29	2.731	4.56	-8.534	-0.287	8.25	3.675	4.57
AC/TZVPP	-7.823	-0.513	7.31	2.770	4.54	-8.556	-0.291	8.27	3.706	4.56
SR/accTZ*	-7.868	-0.645	7.22	2.658	4.56	-8.594	-0.439	8.16	3.565	4.59
SR/QZVPP*	-8.028	-0.645	7.38	2.831	4.55	-8.790	-0.430	8.36	3.784	4.58
SR/SVP	-7.452	-0.385	7.07	2.491	4.58	-8.137	-0.145	7.99	3.405	4.59
AC/SVP	-7.465	-0.378	7.09	2.530	4.56	-8.142	-0.146	8.00	3.422	4.57

* Using the def2-TZVPP optimised geometry

Table 2 Occupied (–IP) and unoccupied (–EA) edge states, fundamental gap (Δ_F), optical gap (Δ_O) and exciton binding energy (EBE) values of $(MgO)_{32}$ as calculated by the different method combinations (TZVPP=def2-TZVPP, SVP=def2-SVP). See table S1 in the supplementary information for BSE/G_0W_0(AC)/def2-TZVPP data starting from PBE rather than B3LYP orbitals.

	G_0W_0					evGW				
	–IP	–EA	Δ_F	Δ_O	EBE	–IP	–EA	Δ_F	Δ_O	EBE
SR/TZVPP	-7.320	-0.365	6.96	3.710	3.24	-7.975	-0.145	7.83	4.538	3.29
AC/TZVPP	-7.333	-0.361	6.97	3.810	3.14	-8.009	-0.152	7.86	4.680	3.18
SR/SVP	-6.989	-0.172	6.82	3.531	3.29	-7.602	0.057	7.66	4.320	3.34
AC/SVP	-7.001	-0.167	6.83	3.691	3.14	-7.618	0.051	7.67	4.494	3.18

Second the effect of the different *GW* approximations and implementations is considered. Going from G_0W_0 to evGW the occupied edge state moves to considerably deeper, more negative, values, the unoccupied edge to noticeably more shallow, less negative values, the fundamental and optical gap increase significantly, while the exciton binding energy stays essentially the same. In contrast, as expected based on the literature, the variation of results calculated between the different *GW* implementations is small. Similarly, the effect of going from ev*GW* to full quasiparticle self-consistent qs*GW* is small other than for the optical gap, which increases by ~0.3 eV, and the exciton binding energy values, which decrease by a similar amount.

The optical gap of the $(MgO)_4$ particles was also calculated using coupled-cluster theory by LR-CCSD calculations. LR-CCSD predicts optical gap values of 3.90 eV and 3.98 eV when using the def2-TZVPP and def2-QZVPP basis-sets, respectively. Comparing these values to the results in Table 1, shows that BSE/G_0W_0 calculations irrespective of the basis-set used significantly underestimate the optical gap relative to LR-CCSD. In contrast, the BSE/evGW optical gap values lie much closer to their LR-CCSD counterparts while BSE/qsGW essentially predicts the same values as LR-CCSD. It should be noted here that both the GW and LR-CCSD calculations ignore vibronic and zero-point motion effects and that as such this is a fair comparison but that the true experimental gap likely will be smaller as a result of such effects.

Based on the comparison with LR-CCSD, BSE/qsGW/def2-QZVPP would be the preferred method to study the electronic and optical properties of the MgO nanoparticles. However, that is in practice not tractable if one wants to study a large number of relatively large particles as the cost of the calculations scales strongly with the basis-set size and qsGW is only implemented in Turbomole in combination with the most computationally expensive spectral representation of GW. Therefore, in the remainder mostly G_0W_0 and evGW calculations will be presented, including calculations with the def2-SVP basis-set. The effect of basis-set while significant is smaller than that of the GW approximation used, optical gap values predicted by evGW/def2-SVP lie much closer to that predicted by LR-CCSD than G_0W_0/def2-QZVPP. More importantly perhaps, all method combinations show the same changes when going from $(MgO)_4$ to $(MgO)_{32}$ and for each of the particles all method combinations predict very similar exciton binding energy values and hence a consistent balance between the fundamental and optical gaps.

Change in edge state positions and optical gap with particle size.

Table 3 gives the edge states, fundamental gap, optical gap and exciton binding energy values predicted by BSE/G_0W_0(AC)/def2-SVP and BSE/evGW(AC)/def2-SVP for a series of cubic and cuboid MgO nanoparticles. Data is shown for $(MgO)_4$, the nx4x4 family, including $(MgO)_{32}$, and the nx5x5 family, which includes $(MgO)_{108}$.

Firstly, concentrating on the optical gap values, it can be observed that all particles studied, bar $(MgO)_4$, have essentially the same optical gap value of 3.6 eV

(G_0W_0) or 4.1 eV (evGW). Analysis of the responsible excitation in terms of the most significant natural transition orbitals shows that for all these particles this involves an excitation where an electron gets excited from the 3-coordinated oxygen corner atoms to the immediately adjacent 4-coordinated magnesium edge atoms (see Fig. 3A). The localised nature of the excitation and the fact that the surface motif responsible is present in all cuboid particles where all edges are at least two unit-cell lengths, probably explains the absence of variation in optical gap with particle size.

Table 3 Occupied (–IP) and unoccupied (–EA) edge states, fundamental gap (Δ_F), optical gap (Δ_O) and exciton binding energy (EBE) values of the different cuboidal nanoparticles as predicted using BSE/G_0W_0(AC)/def2-SVP and BSE/evGW(AC)/def2-SVP.

MgO		G_0W_0					evGW				
		–IP	–EA	Δ_F	Δ_O	EBE	–IP	–EA	Δ_F	Δ_O	EBE
4	(2:2:2)	-7.311	-0.416	6.90	2.362	4.53	-7.984	-0.181	7.80	3.253	4.55
24	(3:4:4)	-6.802	-0.363	6.44	3.574	2.86	-7.429	-0.139	7.29	4.395	2.90
32	(4:4:4)	-6.904	-0.209	6.70	3.599	3.10	-7.524	0.015	7.54	4.409	3.13
40	(5:4:4)	-6.680	-0.229	6.63	3.601	3.03	-7.476	-0.008	7.47	4.403	3.06
48	(6:4:4)	-6.863	-0.200	6.66	3.604	3.06	-7.479	0.023	7.50	4.407	3.09
54	(4:6:6)	-6.535	-0.532	6.00	3.626	2.38	-7.160	-0.306	6.85	4.441	2.41
56	(7:4:4)	-6.853	-0.198	6.66	3.606	3.05	-7.468	0.025	7.49	4.407	3.09
64	(8:4:4)	-6.854	-0.189	6.67	3.609	3.06	-7.469	0.035	7.50	4.412	3.09
72	(4:6:6)	-6.823	-0.206	6.62	3.618	3.00	-7.434	0.017	7.45	4.415	3.04
90	(5:6:6)	-6.650	-0.340	6.31	3.607	2.70	-7.262	-0.119	7.14	4.402	2.70
108	(6:6:6)	-6.703	-0.246	6.46	3.597	2.86	-7.313	-0.022	7.29	4.392	2.90

In contrast to the optical gap, the edge states and by extension also the fundamental gap do change with particle size, even if the picture is confusing. Focussing first on the cubes: $(MgO)_4$, $(MgO)_{32}$ and $(MgO)_{108}$, it can be observed that the occupied edge consistently moves to less negative, shallower, values. The unoccupied edge also moves to less negative, shallower, values when going from $(MgO)_4$ to $(MgO)_{32}$ but then moves to slightly more negative, deeper, values when going to $(MgO)_{108}$. The fundamental gap, finally, consistently gets smaller with increasing edge length and particle size.

For the cuboid nx4x4 and nx5x5 families, where n is even, increasing the length of one of the edges, *e.g.* going from $(MgO)_{32}$ to $(MgO)_{48}$, shift the occupied edge to less negative values, and decreasing the length of one of the edges, *e.g.* going from $(MgO)_{108}$

to $(MgO)_{72}$, shift the occupied edge to more negative values. The unoccupied edge shifts to less negative values with increasing edge length for the nx3x3 family but, just like for the cubes, shifts to more negative values for the nx5x5 family. For the n is odd cuboids, which differ from the cubes and the n is even cuboids in the fact that the corner atoms of the edge are the same (*e.g.* both oxygen atoms) rather than different, similar trends can be observed but the absolute values appear shifted. Just as for the cubes the fundamental gap for the different cuboid families appears to decrease with particle size and edge length. For both the edge states and the fundamental gap, finally, the effect of increasing the edge length appears to decrease in magnitude when one edge becomes much longer than the other two.
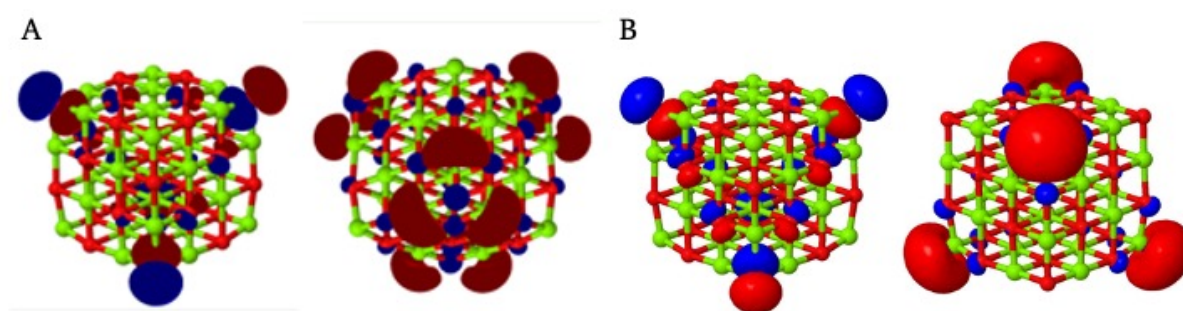
Fig. 3 Leading occupied (A, left) and unoccupied (A, right) natural transition orbitals for the lowest excitation of $(MgO)_{32}$ and the highest occupied (B, left) and lowest unoccupied (B, right) Kohn-Sham orbitals for the same particle. As the calculation was performed using the D_2 instead of the T_d point group, the triply degenerate T_2 excited state is described as a triplet of excited states of B_1, B_2 and B_3 symmetry, the natural transition orbitals of only one is shown in A. Similarly (B, left) is one of three degenerate orbitals.

While the lowest excitation corresponding to the optical gap for all particles involves, as discussed above, the 3-coordinated oxygen corner atoms and the immediately adjacent 4-coordinated magnesium edge atoms, the ground-state Kohn-Sham orbitals from DFT corresponding to the occupied and unoccupied edge states for all cubic and cuboid particles considered are localised on the 3-coordinated oxygen atoms, with minor contributions of the oxygen atoms on the edge or diagonal between these 3-coordinated oxygen atoms, and 3-coordinated magnesium atoms, respectively (see Fig. 3B). The fact that in the lowest excitation the electron gets excited from 4-

coordinated magnesium edge atoms adjacent to the 3-coordinated oxygen corner atoms rather than from the 3-coordinated magnesium corner atoms combined with the fact that the optical gap is much smaller than the fundamental gap for all particles suggests that this excitation is excitonic in character.

Table 4 Occupied (–IP) and unoccupied (–EA) edge states, fundamental gap (Δ_F), optical gap (Δ_O) and exciton binding energy (EBE) values of the different cuboidal nanoparticles with odd-membered faces as predicted using BSE/G_0W_0(AC)/def2-SVP and BSE/evGW(AC)/def2-SVP.

MgO	G_0W_0					evGW				
	–IP	–EA	Δ_F	Δ_O	EBE	–IP	–EA	Δ_F	Δ_O	EBE
18 (3:3:3)	-6.362	-0.772	5.59	3.278	2.31	-6.998	-0.548	6.45	4.127	2.32
27 (4:3:3)	-5.817	-1.225	4.59	3.082	1.51	-6.451	-0.997	5.45	3.950	1.50

Cuboid MgO particles with odd-numbered faces.

Table 4 gives the edge states, fundamental gap, optical gap and exciton binding energy values predicted by BSE/G_0W_0(AC)/def2-SVP and BSE/evGW(AC)/def2-SVP for a series of cuboid MgO nanoparticles of which two of the faces have an odd number of atoms. The same results calculated with def2-TZVPP for the smallest one (($MgO)_{18}$) can be found in Table S2 in the supplementary material. In the previous (TD-)DFT study of MgO nanoparticles it was noted that these odd-numbered faces behaved as if polar, even if extended (100) surfaces are not polar in the conventional sense.[30] Because one odd-membered face has one more magnesium atom than the opposite other odd-membered face and the latter has one more oxygen atom than the former, these particles have a very large dipole moment along the axis of the particle perpendicular to the odd-membered faces (17.3 Debye and 32.6 Debye for $(MgO)_{18}$ and $(MgO)_{27}$, respectively), with the magnitude of the dipole increasing with the particle dimension along that axis. This polarisation in the ground state goes together with a reduction in the optical and fundamental gap of these particles relative to cubes and cuboidal particles lacking these odd-membered faces, where the size of both gaps decreases with the particle dimension along the axis of the particle perpendicular to the odd-membered faces. Analysis of the ground state orbitals from DFT and the most

significant natural transition orbitals from BSE for $(MgO)_{27}$ clearly show the polarisation. The ground state orbital corresponding to the occupied edge state is localised on the central oxygen atom and the four oxygen corner atoms of the oxygen-rich odd-membered face and the orbital for the unoccupied edge is localised over the four magnesium corner atoms and the central magnesium atom of the magnesium-rich odd-membered face, while the most significant natural transition orbitals for the optical gap corresponds to an excitation of an electron from the oxygen atoms of the oxygen-rich odd membered face to the magnesium atoms of the magnesium rich face.

While particles with odd-membered faces larger than $(MgO)_{27}$ were not considered here, the data suggests that for very large particle dimension the fundamental and optical gaps of such particles might go to zero with the particles becoming metallic. However, as discussed below this situation is unlikely to be ever encountered in experiment.
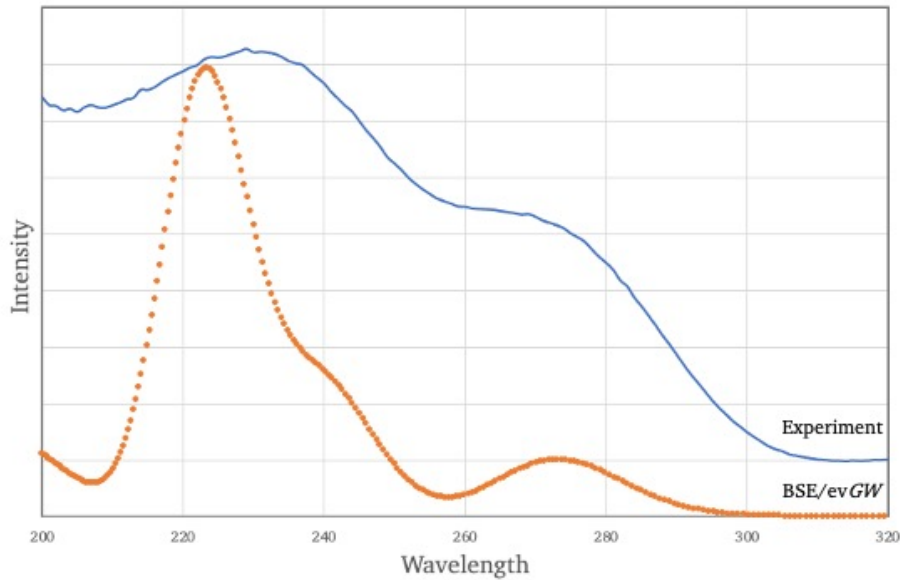

Fig. 4 The vertical excitation spectrum of $(MgO)_{32}$ as predicted using BSE/evGW(SR)/def2-TZVPP (red line) and the experimental measured reflection spectrum of 3 nm MgO particles (blue line). Experimental data taken from reference 10.

Optical spectra of cubic MgO particles.

Fig. 4 shows the vertical excitation spectrum of $(MgO)_{32}$ as predicted using BSE/ev*GW*(SR)/def2-TZVPP, as well as the experimental UV-vis spectrum of 3 nm MgO particles[10] measured by Stankic and co-workers. While the roughly four times difference in size there is a good match between the predicted and experimental spectrum, in line with the observation above that the energy of the lowest exciton is the same for all cuboid particles with even faces and all edges corresponding to at least two unit-cell lengths. All excitations shown in Fig. 4 are 4.6-1.9 eV smaller than the ev*GW*(SR)/def2-TZVPP predicted fundamental gap, suggesting that not only the lowest energy / longest wavelength excitation but all excitations to at least 200 nm are excitonic in character.

The bright excitations were analysed in terms of the most important natural transition orbitals. The lowest bright excitation at 4.54 eV or 273 nm, responsible for the most red-shifted broad peak is, as discussed above, due to an excitation of an electron from the 3-coordinated oxygen corner atoms to the immediately adjacent 4-coordinated magnesium edge atoms (See Fig. 3A). The shoulder at 240 nm is the sum of two bright excitations. The bright excitation at 5.12 eV or 242 nm corresponds to an excitation of an electron from the 4-coordinated oxygen edge atoms to 3-coordinated corner magnesium atoms (see Fig. 5A), while the bright excitation at 5.17 or 240 nm corresponds just like the lowest bright excitation to an excitation of an electron from the 3-coordinated oxygen corner atoms to the adjacent 4-coordinated magnesium edge atoms (see Fig. 5B). The two main contributions to the strongest peak at 220 nm are an excitation at 5.52 eV or 224 nm, corresponding just like the 5.12 eV or 242 nm excitation to an excitation of an electron from the 4-coordinated oxygen edge atoms to 3-coordinated corner magnesium atoms (see Fig. 5C), and an excitation at 5.59 eV or 222 nm, which involves a similar excitation of an electron from now both the 4-coordinated edge and 6-coordinated bulk oxygen atoms to the 3-coordinated corner magnesium atoms (see Fig. 5D). Higher-energy shorter-wavelength bright excitations up to 200 nm display increased contribution of 5- and 6-coordinated oxygen atoms and 4-coordinated magnesium atoms but the 3-/4-coordinated oxygen atoms and 3-coordinated magnesium atoms remain (the) most significant contributors.

Compared to the previous TD-DFT calculations[30] using the range-separated CAM-B3LYP functional the main difference is the predicted character of the excitations responsible for the 240 nm shoulder. TD-CAM-BLYP predicts that one of the excitations contributing to that shoulder corresponds to an excitation of an electron from a 3-coordinated corner oxygen atom to a 3-coordinated corner magnesium atom, something that is not observed in the BSE/evGW predicted spectra to much higher excitation energies / shorter wavelengths.
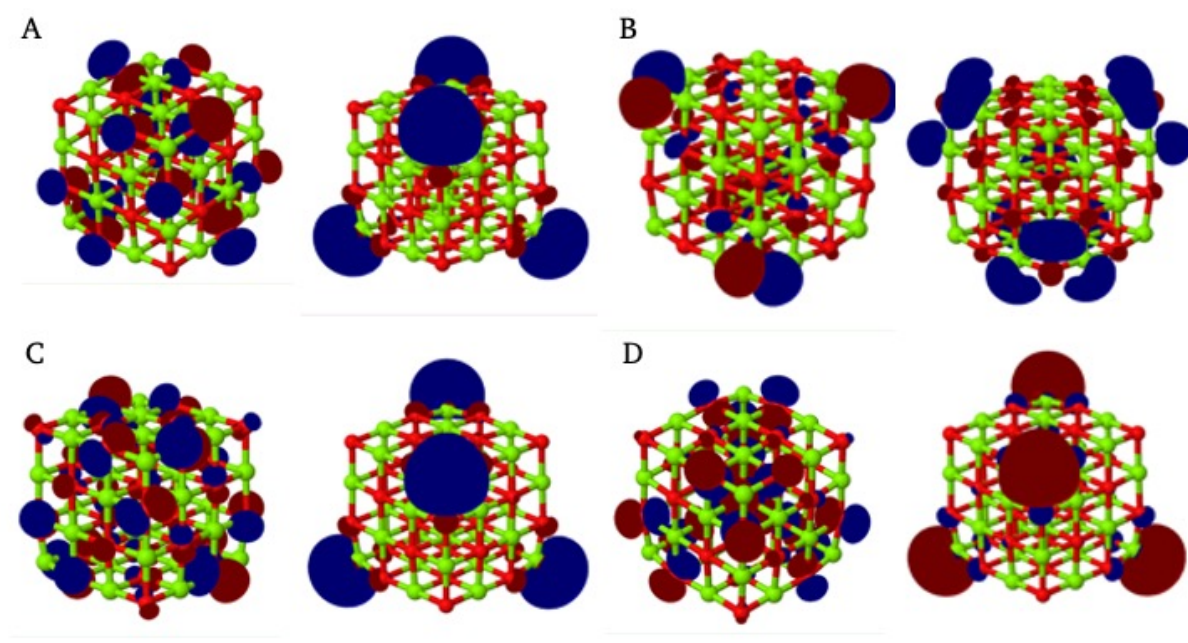
Fig. 5 Leading natural transition orbitals for the 5.12 (A), 5.17 (B), 5.52 (C) and 5.59 (D) eV bright excitations of $(MgO)_{32}$. Similar to Fig. 3. only one of the three degenerate leading natural transition orbitals for each of the excitations is shown.

Beyond MgO

As discussed in the introduction nanoparticles of CaO and SrO grown through chemical vapour deposition show experimentally the same red-shift relative to the bulk in the UV-Vis reflection spectra as MgO nanoparticles. To probe if nanoparticles of such other rocksalt materials display the same physics as that discussed above for MgO nanoparticles the optical and electronic properties of 4x4x4 $(CaO)_{32}$ and $(SrO)_{32}$ cubes were calculated using BSE/G_0W_0 and BSE/evGW, see Table 5.

Table 5 Occupied (–IP) and unoccupied (–EA) edge states, fundamental gap (Δ_F), optical gap (Δ_O) and exciton binding energy (EBE) values of $(CaO)_{32}$ and $(SrO)_{32}$ cubes predicted using BSE/G_0W_0(AC)/def2-TZVPP and BSE/evGW(AC)/def2-TZVPP.

	G_0W_0					evGW				
	–IP	–EA	Δ_F	Δ_O	EBE	–IP	–EA	Δ_F	Δ_O	EBE
CaO (4:4:4)	-5.810	-0.015	5.80	3.079	2.72	-6.363	0.120	6.48	3.736[*]	2.75
SrO (4:4:4)	-5.270	-0.042	5.23	2.640	2.59	-5.805	0.086	5.89	3.278	2.61

[*] The lowest excited-state for $(CaO)_{32}$ as calculated using BSE/evGW(AC)/def2-TZVPP is symmetry forbidden. The 3.736 eV excitation is the lowest optically allowed excitation, second lowest overall. The lowest BSE/evGW(AC)/def2-TZVPP excitation belongs to the A irrep for T_d and has an excitation energy of 3.634 eV and an EBE value of 2.85 eV.

As can be seen from Table 5, the lowest excitations of these CaO and SrO particles are just as for their MgO counterparts excitonic in character with predicted exciton binding energies of more than 2 eV. Visualisation of the natural transition orbitals for these particles also show that, just in the case of MgO particles, the lowest energy excitons are strongly localised around the corner atoms, see Fig. S1 in the supporting information. Finally, the predicted optical gap values are comparable to experimentally measured lowest excitation energies of CaO (3.5 eV)[11] and SrO (3.7 eV)[12] nanoparticles.

Discussion

The BSE/evGW calculations show in line with the experimental work by Stankic and others that the optical gap of MgO nanoparticles is much smaller than that of the bulk and that such particles absorb light in the middle ultraviolet, 200-300 nm, where the bulk does not. The excitations responsible or the light absorption in that wavelength range are all predicted to be excitonic in character as the predicted fundamental gap of all particles considered, excluding those with odd-membered faces, is larger than 200 nm. The lowest exited-state in all cases bar the smallest nanoparticles corresponds to a well-localised exciton involving the 3-coordinated oxygen corner atoms and their immediate 4-coordinated magnesium atoms, where the optical gap does not change with particle size. These MgO nanoparticles hence do not behave as quantum dots but rather as defective insulators, where light absorption at longer wavelengths / lower energies than the bulk is due to excitations of electrons between what are essentially surface defects.

As discussed above the edge states and the fundamental gap in contrast to the optical gap do change with particle size. The relevant orbitals are again relatively localised but more delocalised than the excited state associated with the optical gap. The origin of the variation of these electronic properties with particle size is unknown. Perhaps more interestingly is the fact that the nature of the variation is unexpected. The occupied edge state is found to move to shallower values, the unoccupied edge to deeper values and hence the fundamental gap decreases with particle size. The bulk fundamental gap cannot be calculated with the same exact set-up as used here for the particles. However, literature prediction of the fundamental gap of bulk MgO using G_0W_0 range from 7.5-8 eV[57-61] and for qsGW a value of 8.69 eV has been reported by Lambrecht and co-workers[62] (in all cases, like the GW calculations here, ignoring vibronic and zero point motion effects, the inclusion of the former brings the qsGW values for the bulk closer to the experimental value of 7.8 eV[63-64]). Comparing these bulk values from the literature to the G_0W_0 and evGW reported here for the nanoparticles here than the nanoparticles (i) have smaller fundamental gaps than bulk MgO, (ii) the nanoparticle edge states likely lie within the fundamental gap of bulk MgO, and (iii) that upon increasing the particle size the fundamental gap appears to diverge away from the bulk value rather than converge towards it. While these observations are by definition is based on a limited range of particle sizes, *e.g.* the next cube has 232 MgO formula units and hence for the moment beyond the horizon of what can be achieved with the GW implementation, it suggests that even for (macroscopically) large particles the corner atoms fix the edge states and the fundamental gap. That is even if this is experimentally unobservable by photoelectron spectroscopy due the relatively very small number of such corner atoms in large particles.

It turns out to be impossible to predict the $(MgO)_{108}$ spectrum using BSE/evGW, even when using the def2-SVP basis-set, due to the very large memory and disk-space requirements to calculate more than just the lowest excited states for this particle. However, it stands to reason that the observed trend in the intensities of the peaks in the experimental reflection spectra, where going from 3 to 10 nm particles the relative intensity of the 270 and 240 nm shoulders/peaks decreases and that of 220 nm peak

increases, finds its origin in the fact that the most red-shifted peaks involve excitations localised on exclusively 3-coordinated corner and 4-coordinated edge atoms while the 220 nm peak also involve 5-coordinated terrace and 6-coordinated bulk atoms and that when increasing the particle size the number of corner and edge atoms relative to surface and bulk atoms decreases. For the same reason and in analogy to the discussion above for the fundamental gap, even for macroscopically large MgO particles the true optical gap would likely be the same as that predicted here for nanoparticles but the optical gap observed in experiment would probably be the bulk value.

The exciton binding energy decreases with particle size, driven by the reduction in the fundamental gap with particle size. In the case of pure cubes extrapolation to the infinite particle limit by plotting the BSE/evGW/def2-SVP exciton binding energy of the lowest energy exciton of the three cubes against the inverse of their edge lengths yields a value of 2.4 eV. This value is more than an order of magnitude larger than the binding energy of the n=1 bulk exciton, 80 meV,[63-64] which is in line with the former probably[65] being a Wannier-Mott exciton while the lowest exciton in the nanoparticles, as discussed, is much more localised and hence more like a Frenkel exciton.
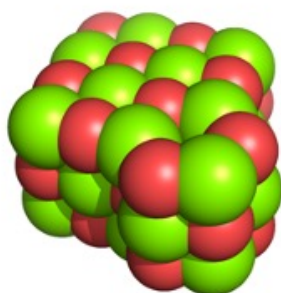
Fig. 6 Structure of the alternative structure considered for $(MgO)_{27}$, the global minimum as proposed by Dixon and co-workers.[21]

The nanoparticles with odd-membered faces have rather different optical and electronic properties relative to their counterparts that only have even-membered faces. However, particles displaying such odd-membered surfaces are unlikely to be observed in experiment as the same ground-state dipole moment that gives rise to these different optical and electronic properties also destabilises them energetically. Previous global optimisation studies find that while for $(MgO)_{18}$ the cuboidal rocksalt structure is still

the predicted global minimum, as it is for particles with only even-membered faces (*i.e.* $(MgO)_{24}$, $(MgO)_{32}$ and $(MgO)_{40}$), for $(MgO)_{27}$ a reconstructed cuboidal structure with a much reduce ground-state dipole moment (0.3 instead of 32.6 Debye) is found to be more stable[21] (see Fig. 6). As expected this reconstructed $(MgO)_{27}$ particle also has a larger optical gap (4.48 eV instead of 3.95 eV when calculated with BSE/evGW(AC)/def2-SVP, see table S3 in the supporting information), which is similar to that of the cubic particles with even-membered faces. In analogy to classically polar surfaces, these particles with odd-membered surfaces can thus be thought to reconstruct to eliminate the large dipole moment and in the process also eliminate their more out of kilter optical properties.

Finally, while this paper studies primarily MgO nanoparticles, the same physics is likely in play in nanoparticles of other oxides. Indeed, as mentioned in the introduction nanoparticles of CaO and SrO have experimentally been observed to display the same red-shift relative to the bulk as MgO nanoparticles and BSE/GW calculations discussed above confirm that for these materials the lowest energy excitations are excitonic in nature and strongly localised around the corner atoms of the nanoparticles. Comparing the BSE/evGW predicted optical gap for the nanoparticles with the experimental excitation energy of the lowest exciton peak in bulk CaO (7 eV)[66] and SrO (5.7 eV),[67-69] confirms the bulk to nanoparticle red shift for these materials. As noted above for MgO, an exact one-to-one comparison to properties predicted for the bulk is difficult, but the BSE/G_0W_0/PBE optical gap values predicted for the CaO and SrO nanoparticles (see table S4) are also indeed significantly smaller than those extracted from the results of periodic BSE/G_0W_0/PBE calculations from the literature.[60, 70] Interestingly, a comparison of the fundamental gap predicted for bulk CaO[60, 71] and SrO,[70-71] using G_0W_0/PBE, and the equivalent fundamental gap of the nanoparticles shows that they are more similar than for MgO, especially in the case of SrO, for which the G_0W_0/PBE fundamental gap (4.85 eV) is virtually identical to that predicted for the bulk. While the lowest energy excitons for nanoparticles of these materials remain clearly localised around the particles' corner atoms and the optical properties thus governed by the presence of these low-coordinated atoms, the edge states appear less tied down.

Conclusions

ev*GW*-BSE calculations on realistic oxide nanoparticles such as those made from MgO are found to be computationally tractable and using such calculations it is demonstrated that the optical and electronic properties of MgO nanoparticles are governed by the presence of low-coordinated atoms on their surfaces, in other words are surface defect states. States localised on these corner and edge atoms are responsible for the occupied and unoccupied edge states, *i.e.* the ionisation potential and the electron affinity, of the particle, and thus the magnitude of the fundamental gap, as well as the lowest excited states and thus the size of the optical gap. As a result the optical gap of all cuboidal rocksalt MgO nanoparticles bar the absolute smallest and particles with odd membered faces is predicted to be essentially the same and to not vary with the particle size. By extrapolation it can be assumed that the same holds true for macroscopic MgO particles, even if this might be hard to observe experimentally due to the much smaller surface to volume ratio for such particles. The BSE/ev*GW* spectrum predicted for $(MgO)_{32}$ agrees well with the experimental spectra for MgO nanoparticles reported in the literature.

Nanoparticles with odd membered faces are predicted to have reduced optical gaps and display large ground state dipole moments perpendicular to the odd membered faces. The presence of such large dipole moments destabilises these particles relative to particles that lack odd membered faces and hence can be argued to reconstruct to reduce the dipole moments, akin to what happens in the case of polar surfaces.

Finally, calculations on CaO and SrO nanoparticles show that they display the same physics as MgO nanoparticles with the lowest energy excitations corresponding to excitons localised on the particles' corners. Nanoparticles of MgO are thus not unique in having electronic and optical properties governed by surface states instead of quantum confinement effects. In fact, the behaviour observed for MgO appears typical of nanoparticles of all alkaline earth oxides and perhaps many other oxides.

Acknowledgements

References

1.	Efros, A. L.; Brus, L. E., Nanocrystal Quantum Dots: From Discovery to Modern Development. *ACS Nano* **2021**, *10.1021/acsnano.1c01399*.

2.	Brus, L., Electronic Wave Functions in Semiconductor Clusters: Experiment and Theory. *The Journal of Physical Chemistry* **1986**, *90*, 2555-2560.

3.	Brus, L. E., Electron–Electron and Electron-Hole Interactions in Small Semiconductor Crystallites: The Size Dependence of the Lowest Excited Electronic State. *The Journal of Chemical Physics* **1984**, *80*, 4403-4409.

4.	Yu, W. W.; Peng, X., Formation of High-Quality Cds and Other II–VI Semiconductor Nanocrystals in Noncoordinating Solvents: Tunable Reactivity of Monomers. *Angewandte Chemie International Edition* **2002**, *41*, 2368-2371.

5.	Murray, C. B.; Norris, D. J.; Bawendi, M. G., Synthesis and Characterization of Nearly Monodisperse CdE (E = Sulfur, Selenium, Tellurium) Semiconductor Nanocrystallites. *Journal of the American Chemical Society* **1993**, *115*, 8706-8715.

6.	Peng, X.; Wickham, J.; Alivisatos, A. P., Kinetics of II-VI and III-V Colloidal Semiconductor Nanocrystal Growth: "Focusing" of Size Distributions. *Journal of the American Chemical Society* **1998**, *120*, 5343-5344.

7.	Cademartiri, L.; Montanari, E.; Calestani, G.; Migliori, A.; Guagliardi, A.; Ozin, G. A., Size-Dependent Extinction Coefficients of Pbs Quantum Dots. *Journal of the American Chemical Society* **2006**, *128*, 10337-10346.

8.	Hines, M. A.; Scholes, G. D., Colloidal PbS Nanocrystals with Size-Tunable near-Infrared Emission: Observation of Post-Synthesis Self-Narrowing of the Particle Size Distribution. *Advanced Materials* **2003**, *15*, 1844-1849.

9.	Murray, C. B.; Sun, S.; Gaschler, W.; Doyle, H.; Betley, T. A.; Kagan, C. R., Colloidal Synthesis of Nanocrystals and Nanocrystal Superlattices. *IBM J. Res. Dev.* **2001**, *45*, 47–56.

10.	Stankic, S.; Müller, M.; Diwald, O.; Sterrer, M.; Knözinger, E.; Bernardi, J., Size-Dependent Optical Properties of Mgo Nanocubes. *Angewandte Chemie International Edition* **2005**, *44*, 4917-4920.

11.	Stankic, S.; Bernardi, J.; Diwald, O.; Knözinger, E., Optical Surface Properties and Morphology of Mgo and Cao Nanocrystals. *The Journal of Physical Chemistry B* **2006**, *110*, 13866-13871.

12.	Stankic, S.; Bernardi, J.; Diwald, O.; Knözinger, E., Photoexcitation of Local Surface Structures on Strontium Oxide Grains. *The Journal of Physical Chemistry C* **2007**, *111*, 8069-8074.

13.	Cohen, M. L.; Lin, P. J.; Roessler, D. M.; Walker, W. C., Ultraviolet Optical Properties and Electronic Band Structure of Magnesium Oxide. *Physical Review* **1967**, *155*, 992-996.

14.   Roessler, D. M.; Walker, W. C., Spin-Orbit Splitting of the Gamma Exciton in MgO. *Physical Review Letters* **1966**, *17*, 319-320.

15.   Spanó, E.; Hamad, S.; Catlow, C. R. A., Computational Evidence of Bubble ZnS Clusters. *The Journal of Physical Chemistry B* **2003**, *107*, 10337-10340.

16.   Spanó, E.; Hamad, S.; Catlow, C. R. A., ZnS Bubble Clusters with Onion-Like Structures. *Chemical Communications* **2004**, 864-865.

17.   Hamad, S.; Catlow, C. R. A.; Spanó, E.; Matxain, J. M.; Ugalde, J. M., Structure and Properties of Zns Nanoclusters. *The Journal of Physical Chemistry B* **2005**, *109*, 2703-2709.

18.   Sanville, E.; Burnin, A.; BelBruno, J. J., Experimental and Computational Study of Small (N = 1–16) Stoichiometric Zinc and Cadmium Chalcogenide Clusters. *The Journal of Physical Chemistry A* **2006**, *110*, 2378-2386.

19.   Zwijnenburg, M. A., Optical Excitations in Stoichiometric Uncapped ZnS Nanostructures. *Nanoscale* **2011**, *3*, 3780-3787.

20.   Roberts, C.; Johnston, R. L., Investigation of the Structures of MgO Clusters Using a Genetic Algorithm. *Physical Chemistry Chemical Physics* **2001**, *3*, 5024-5034.

21.   Chen, M.; Felmy, A. R.; Dixon, D. A., Structures and Stabilities of $(MgO)_N$ Nanoclusters. *The Journal of Physical Chemistry A* **2014**, *118*, 3136-3146.

22.   Escher, S. G. E. T.; Lazauskas, T.; Zwijnenburg, M. A.; Woodley, S. M., Synthesis Target Structures for Alkaline Earth Oxide Clusters. *Inorganics* **2018**, *6*, 29.

23.   Wu, M.-C.; Truong, C. M.; Goodman, D. W., Electron-Energy-Loss-Spectroscopy Studies of Thermally Generated Defects in Pure and Lithium-Doped MgO(100) Films on Mo(100). *Physical Review B* **1992**, *46*, 12688-12694.

24.   Kolmakov, A.; Stultz, J.; Goodman, D. W., Characterization of Surface Defects on MgO Thin Films by Ultraviolet Photoelectron and Metastable Impact Electron Spectroscopies. *The Journal of Chemical Physics* **2000**, *113*, 7564-7570.

25.   Cox, P. A.; Williams, A. A., Surface Excitons on Ionic Crystals. *Surface Science Letters* **1986**, *175*, L782-L786.

26.   Trevisanutto, P. E.; Sushko, P. V.; Shluger, A. L.; Beck, K. M.; Henyk, M.; Joly, A. G.; Hess, W. P., A Mechanism of Photo-Induced Desorption of Oxygen Atoms from MgO Nano-Crystals. *Surface Science* **2005**, *593*, 210-220.

27.   Müller, M.; Stankic, S.; Diwald, O.; Knözinger, E.; Sushko, P. V.; Trevisanutto, P. E.; Shluger, A. L., Effect of Protons on the Optical Properties of Oxide Nanostructures. *Journal of the American Chemical Society* **2007**, *129*, 12491-12496.

28.   McKenna, K. P.; Koller, D.; Sternig, A.; Siedl, N.; Govind, N.; Sushko, P. V.; Diwald, O., Optical Properties of Nanocrystal Interfaces in Compressed MgO Nanopowders. *ACS Nano* **2011**, *5*, 3003-3009.

29.   Sternig, A.; Koller, D.; Siedl, N.; Diwald, O.; McKenna, K., Exciton Formation at Solid–Solid Interfaces: A Systematic Experimental and Ab Initio Study on Compressed MgO Nanopowders. *The Journal of Physical Chemistry C* **2012**, *116*, 10103-10112.

30.   Wobbe, M. C. C.; Kerridge, A.; Zwijnenburg, M. A., Optical Excitation of MgO Nanoparticles; a Computational Perspective. *Physical Chemistry Chemical Physics* **2014**, *16*, 22052-22061.

31.   Peach, M. J. G.; Benfield, P.; Helgaker, T.; Tozer, D. J., Excitation Energies in Density Functional Theory: An Evaluation and a Diagnostic Test. *The Journal of Chemical Physics* **2008**, *128*, 044118.

32.   Tozer, D. J.; Amos, R. D.; Handy, N. C.; Roos, B. O.; Serrano-Andres, L., Does Density Functional Theory Contribute to the Understanding of Excited States of Unsaturated Organic Compounds? *Molecular Physics* **1999**, *97*, 859-868.

33.   Baerends, E. J.; Gritsenko, O. V.; van Meer, R., The Kohn–Sham Gap, the Fundamental Gap and the Optical Gap: The Physical Meaning of Occupied and Virtual Kohn–Sham Orbital Energies. *Physical Chemistry Chemical Physics* **2013**, *15*, 16408-16425.

34.   Sushko, P. V.; Gavartin, J. L.; Shluger, A. L., Electronic Properties of Structural Defects at the MgO (001) Surface. *The Journal of Physical Chemistry B* **2002**, *106*, 2269-2276.

35.   McKenna, K. P.; Shluger, A. L., First-Principles Calculations of Defects near a Grain Boundary in MgO. *Physical Review B* **2009**, *79*, 224116.

36.   McKenna, K. P.; Shluger, A. L., Electron and Hole Trapping in Polycrystalline Metal Oxide Materials. *Proceedings of the Royal Society A: Mathematical, Physical and Engineering Sciences* **2011**, *467*, 2043-2053.

37.   Hedin, L., New Method for Calculating the One-Particle Green's Function with Application to the Electron-Gas Problem. *Physical Review* **1965**, *139*, A796-A823.

38.   Aryasetiawan, F.; Gunnarsson, O., Thegwmethod. *Reports on Progress in Physics* **1998**, *61*, 237-312.

39.   Golze, D.; Dvorak, M.; Rinke, P., The GW Compendium: A Practical Guide to Theoretical Photoemission Spectroscopy. *Frontiers in Chemistry* **2019**, *7*.

40.   Salpeter, E. E.; Bethe, H. A., A Relativistic Equation for Bound-State Problems. *Physical Review* **1951**, *84*, 1232-1242.

41.   Strinati, G., Application of the Green's Functions Method to the Study of the Optical Properties of Semiconductors. *La Rivista del Nuovo Cimento (1978-1999)* **1988**, *11*, 1-86.

42.   Blase, X.; Duchemin, I.; Jacquemin, D.; Loos, P.-F., The Bethe–Salpeter Equation Formalism: From Physics to Chemistry. *The Journal of Physical Chemistry Letters* **2020**, *11*, 7371-7382.

43.   Vosko, S. H.; Wilk, L.; Nusair, M., Accurate Spin-Dependent Electron Liquid Correlation Energies for Local Spin Density Calculations: A Critical Analysis. *Canadian Journal of Physics* **1980**, *58*, 1200-1211.

44.   Lee, C.; Yang, W.; Parr, R. G., Development of the Colle-Salvetti Correlation-Energy Formula into a Functional of the Electron Density. *Physical Review B* **1988**, *37*, 785-789.

45.   Becke, A. D., Density-Functional Thermochemistry. III. The Role of Exact Exchange. *The Journal of Chemical Physics* **1993**, *98*, 5648-5652.

46.   Stephens, P. J.; Devlin, F. J.; Chabalowski, C. F.; Frisch, M. J., Ab Initio Calculation of Vibrational Absorption and Circular Dichroism Spectra Using Density Functional Force Fields. *The Journal of Physical Chemistry* **1994**, *98*, 11623-11627.

47.   Grimme, S.; Antony, J.; Ehrlich, S.; Krieg, H., A Consistent and Accurate Ab Initio Parametrization of Density Functional Dispersion Correction (DFT-D) for the 94 Elements H-Pu. *The Journal of Chemical Physics* **2010**, *132*, 154104.

48.   Grimme, S.; Ehrlich, S.; Goerigk, L., Effect of the Damping Function in Dispersion Corrected Density Functional Theory. *Journal of Computational Chemistry* **2011**, *32*, 1456-1465.

49.   Weigend, F.; Ahlrichs, R., Balanced Basis Sets of Split Valence, Triple Zeta Valence and Quadruple Zeta Valence Quality for H to Rn: Design and Assessment of Accuracy. *Physical Chemistry Chemical Physics* **2005**, *7*, 3297-3305.

50.   van Setten, M. J.; Weigend, F.; Evers, F., The Gw-Method for Quantum Chemistry Applications: Theory and Implementation. *Journal of Chemical Theory and Computation* **2013**, *9*, 232-246.

51.   Gui, X.; Holzer, C.; Klopper, W., Accuracy Assessment of Gw Starting Points for Calculating Molecular Excitation Energies Using the Bethe–Salpeter Formalism. *Journal of Chemical Theory and Computation* **2018**, *14*, 2127-2136.

52.   Holzer, C.; Klopper, W., Ionized, Electron-Attached, and Excited States of Molecular Systems with Spin–Orbit Coupling: Two-Component Gw and Bethe–Salpeter Implementations. *The Journal of Chemical Physics* **2019**, *150*, 204116.

53.   Perdew, J. P.; Burke, K.; Ernzerhof, M., Generalized Gradient Approximation Made Simple. *Physical Review Letters* **1996**, *77*, 3865-3868.

54.   Krause, K.; Klopper, W., Implementation of the Bethe–Salpeter Equation in the Turbomole Program. *Journal of Computational Chemistry* **2017**, *38*, 383-388.

55.   Martin, R. L., Natural Transition Orbitals. *The Journal of Chemical Physics* **2003**, *118*, 4775-4777.

56.   Balasubramani, S. G., et al., Turbomole: Modular Program Suite for Ab Initio Quantum-Chemical and Condensed-Matter Simulations. *The Journal of Chemical Physics* **2020**, *152*, 184107.

57.   Cappellini, G.; Bouette-Russo, S.; Amadon, B.; Noguera, C.; Finocchi, F., Structural Properties and Quasiparticle Energies of Cubic SrO, MgO and $SrTiO_3$. *Journal of Physics: Condensed Matter* **2000**, *12*, 3671-3688.

58.   Schleife, A.; Fuchs, F.; Furthmüller, J.; Bechstedt, F., First-Principles Study of Ground- and Excited-State Properties of MgO, ZnO, and CdO Polymorphs. *Physical Review B* **2006**, *73*, 245212.

59.   Rinke, P.; Schleife, A.; Kioupakis, E.; Janotti, A.; Rödl, C.; Bechstedt, F.; Scheffler, M.; Van de Walle, C. G., First-Principles Optical Spectra for F Centers in MgO. *Physical Review Letters* **2012**, *108*, 126404.

60.   Nejatipour, H.; Dadsetani, M., Excitonic Effects in the Optical Properties of Alkaline Earth Chalcogenides from First-Principles Calculations. *Physica Scripta* **2015**, *90*, 085802.

61.   Gao, W.; Xia, W.; Gao, X.; Zhang, P., Speeding up Gw Calculations to Meet the Challenge of Large Scale Quasiparticle Predictions. *Scientific Reports* **2016**, *6*, 36849.

62.   Lambrecht, W. R. L.; Bhandari, C.; van Schilfgaarde, M., Lattice Polarization Effects on the Screened Coulomb Interaction W of the GW Approximation. *Physical Review Materials* **2017**, *1*, 043802.

63.   Roessler, D. M.; Walker, W. C., Electronic Spectrum and Ultraviolet Optical Properties of Crystalline MgO. *Physical Review* **1967**, *159*, 733-738.

64.   Schmidt-Grund, R.; Carstens, A.; Rheinländer, B.; Spemann, D.; Hochmut, H.; Zimmermann, G.; Lorenz, M.; Grundmann, M.; Herzinger, C. M.; Schubert, M., Refractive Indices and Band-Gap Properties of Rocksalt $Mg_xZn_{1-x}O$ ($0.68 \leqslant X \leqslant 1$). *Journal of Applied Physics* **2006**, *99*, 123701.

65.   Begum, V.; Gruner, M. E.; Vorwerk, C.; Draxl, C.; Pentcheva, R., Theoretical Description of Optical and X-Ray Absorption Spectra of Mgo Including Many-Body Effects. *arXiv preprint arXiv:2012.08960* **2020**.

66.   Whited, R. C.; Walker, W. C., Exciton Spectra of CaO and MgO. *Physical Review Letters* **1969**, *22*, 1428-1430.

67.   Rao, A. S.; Kearney, R. J., Logarithmic Derivative Reflectance Spectra of BaO and SrO. *physica status solidi (b)* **1979**, *95*, 243-250.

68.   Summers, G. P., Optical Absorption and Emission near the Band Edge of SrO. *Physical Review B* **1979**, *20*, 5275-5279.

69.   Feldbach, E.; Kink, R.; Kirm, M.; Lushchik, A.; Lushchik, C.; Lôhmus, A.; Maaroos, A.; Martinson, I., Electronic Excitations and Uv Luminescence in SrO Crystals at 8 K. *Chemical physics letters* **1995**, *241*, 597-602.

70.   Ma, C.; Liu, T.; Chang, Q., Study on the Electronic Structures and Optical Absorption of F Center in the Sro Crystal with G_0W_0–BSE. *Computational and Theoretical Chemistry* **2016**, *1080*, 79-83.

71.   Riefer, A.; Fuchs, F.; Rödl, C.; Schleife, A.; Bechstedt, F.; Goldhahn, R., Interplay of Excitonic Effects and Van Hove Singularities in Optical Spectra: CaO and AlN Polymorphs. *Physical Review B* **2011**, *84*, 075218.